

# Development of sputtered nitrogen-doped $\text{Li}_{1+x}\text{Al}_x\text{Ge}_{2-x}(\text{PO}_4)_3$ thin films for solid state batteries

Tayebeh Mousavi, Isabel Slattery, Ben Jagger, Junliang Liu, Susannah Speller, Chris Grovenor

Department of Materials, University of Oxford, Parks Road, Oxford, OX1 3PH, UK

## Abstract

Nitrogen-doped  $\text{Li}_{1+x}\text{Al}_x\text{Ge}_{2-x}(\text{PO}_4)_3$  (LAGP) thin films were prepared by magnetron sputtering in a mixture of  $\text{Ar}+\text{N}_2$  using an LAGP powder target. The as-deposited films were amorphous, but could be crystallised into the NASICON LAGP phase after annealing at temperatures above  $550\text{ }^\circ\text{C}$ . The introduction of nitrogen to the sputtering gas has two effects on the deposited films; incorporation of a low concentration of nitrogen into the LAGP phase but also reduction of the rate of deposition. The former leads to improvements in Li ion conductivity whereas the latter can cause porosity and discontinuities in the films and limits their application in solid state devices. Up to 23% nitrogen in the sputtering gas the first effect is dominant and the total ionic conductivity improves without introducing morphological defects. However if the nitrogen content is increased further, the porosity decreases the measured conductivity. Optimised nitrogen doping in the sputtered LAGP films results in ionic conductivities as high as  $2.3\times 10^{-4}\text{ S cm}^{-1}$  in films only  $1\text{ }\mu\text{m}$  thick (2.7 times higher than undoped LAGP films) and activation energies below  $0.38\text{ eV}$ .

**Keywords:** Solid electrolyte, Thin films, N-doped LAGP, Sputtering

## Introduction

Solid-state lithium batteries may offer a solution to the safety issues being experienced in current lithium ion batteries containing flammable organic electrolytes [1], [2]. The properties of the solid electrolyte is the key to the overall performance of these batteries, and the NASICON-type glass-ceramic  $\text{Li}_{1+x}\text{Al}_x\text{Ge}_{2-x}(\text{PO}_4)_3$  (LAGP) is a promising solid electrolyte being considered for this role because of its relatively high ionic conductivity, reasonably wide potential window, chemical stability and adequate mechanical properties [3], [4]. Bulk LAGP electrolyte ceramics are normally fabricated by solid-state processing strategies resulting in room temperature ionic conductivity values in the range  $3.3\text{--}6.7\times 10^{-4}\text{ S cm}^{-1}$  [3]–[6]. However it is difficult using solid-state processing to prepare the large area electrolyte layers thinner than  $10\text{ }\mu\text{m}$  required to achieve high overall energy densities, and so thin film deposition

methods have recently been explored to manufacture the thinner layers of solid electrolytes needed for optimising battery performance [7]. Sputtering has been used to fabricate thin films of several solid electrolyte materials, in particular LiPON [8], LLZO [9], and LAGP [10], [11]. Recently we optimised the sputtering and post annealing parameters to fabricate 1  $\mu\text{m}$  LAGP films with ionic conductivities as high as  $10^{-4} \text{ S cm}^{-1}$  [12], comparable to those reported for bulk ceramic samples fabricated by solid-state processing at high temperatures [3], [4].

It is well known that the addition of nitrogen to solid electrolyte compounds can decrease the activation energy for ionic diffusion [13], [14], and this approach was successfully used to incorporate N into thin-film LiPON electrolytes by reactive RF magnetron sputtering from lithium orthophosphate ( $\text{Li}_3\text{PO}_4$ ) targets [15]. The ionic conductivity of these films significantly increases with the atomic percentage (at.%) of N incorporated in the material, while the activation energy for Li diffusion correspondingly decreases. Bates et al showed a substantial increase in ionic conductivity at  $25^\circ\text{C}$  when the N content increases from 0 at. % ( $\sigma = 7 \times 10^{-8} \text{ S cm}^{-1}$ ) to the highest concentration achieved of 6 at. % ( $\sigma = 3.3 \times 10^{-6} \text{ S cm}^{-1}$ ) [15]. Based on the interpretation of XPS results from nitrogen-containing bulk sodium metaphosphate glasses, similar analysis of these LiPON films indicated the presence of two nitrogen environments that were assigned to nitrogen bound to either two or three phosphate tetrahedra [15], [16]. This assignment has been widely accepted, and it has been proposed that the conductivity enhancement by nitrogen doping is due to the bridging of phosphate tetrahedra into a more strongly cross-linked glassy structure [17].

However, Wang et al produced crystalline LiPON with the  $\gamma\text{-Li}_3\text{PO}_4$  structure and interpreted their XPS data as showing that the majority of the N was bound to only one phosphate tetrahedron, with a minor contribution from Li – P disorder resulting in N bound to two tetrahedra. The  $\text{N}_{1s}$  XPS spectrum from this material appears similar to that reported by Bates et al, which raises questions about the validity of the original peak assignment [15], [18]. Additionally, sputtered LiPON films have very different starting materials and processing conditions to bulk glasses, and a direct comparison between XPS spectra from the two may not be appropriate [19]. Lacivita et al investigated nitrogen-incorporation in LiPON through combined experimental and computational methods and also determined that the nitrogen is either apical or bridging, and in these locations being covalently bonded to one or two phosphate groups respectively [20]. They suggested that these bridging nitrogen atoms are covalently bonded to two phosphorus atoms and interact less strongly with the mobile  $\text{Li}^+$  ions than apical nitrogen or oxygen atoms.

Since the development of LiPON, reactive nitrogen sputtering of electrolytes has been explored for other systems, including LiBON [21], LiSON [22], LiSPON [23], LiBPON [17], [24], LiSiPON [25], [26] and LiAlTiPON [27]. LATP thin films have been fabricated by magnetron sputtering in nitrogen, giving ionic conductivities as high as  $1.22 \times 10^{-5} \text{ S cm}^{-1}$  at room temperature [27]. A similar XPS analysis to that described above was used to suggest that the high ionic conductivity of these films is due to the formation of double and triply coordinated nitrogen in the phosphate network and the mixed anion effect which reduces the electrostatic energy [27]. LiSiPON thin films display an even higher ionic conductivity of  $2 \times 10^{-5} \text{ S cm}^{-1}$  ( $E_a = 0.45 \text{ eV}$ ) at room temperature, which is attributed to a combination of mixed-former, amorphization and nitridation effects [26].

Here we focus on the fabrication of polycrystalline N-doped LAGP thin films. The microstructure and ionic conductivity of these films have been characterized to provide an understanding of the effects of nitrogen doping on the microstructure and ionic conductivity in LAGP(N) films.

## Experimental methods

N-doped LAGP thin films were grown by RF magnetron sputtering. The sputtering parameters were chosen based on our previous work [12] on the deposition of undoped LAGP films, where the processing parameters have been optimised for high deposition rates and the production of chemically uniform films with composition similar to that of the target. These parameters include a power density of  $2.2 \text{ W/cm}^2$ , total gas pressure of  $5.3 \times 10^{-3} \text{ mbar}$  and sputtering time of 6 hrs. These same conditions were used for all the films described here. The sputtering target was prepared from commercial LAGP powder from MTI with nominal composition  $\text{Li}_{1.5}\text{Al}_{0.5}\text{Ge}_{1.5}(\text{PO}_4)_3$ . The sputtering gas was an Ar/N<sub>2</sub> mix (0-30 vol.% N<sub>2</sub>) with a total flow of 50 sccm. (0001)-Al<sub>2</sub>O<sub>3</sub> substrates were cleaned ultrasonically for 10 mins in isopropanol before being mounted 5 cm from the target. The schematic image of our sputtering set up can be found in [28][29]. Based on our previous work, post-deposition annealing was carried out at temperatures between 550 and 750 °C, since crystallisation of the amorphous as-sputtered films was observed to start at around 550 °C and highly crystalline films with the highest density were found at 700 °C [12]. During the heat-treatment process, the samples were surrounded by an excess of the starting LAGP powder to limit the loss of volatile lithium.

Deposited and annealed thin films were characterized by X-ray diffraction (XRD) using Cu K $\alpha$  radiation in a Panalytical Empyrean instrument at 40 V and 40 mA. The microstructure of the films was characterized by scanning electron microscopy (SEM-Zeiss EVO MA10, and

Zeiss Merlin), and compositional analysis was carried out by Energy Dispersive X-ray analysis (EDX) using an Oxford Instruments X-Max 150 silicon drift detector. The accelerating voltage for the EDX analysis was 15 kV. Cross-sections of the annealed films were prepared for chemical analysis by a Plasma Focused Ion Beam Scanning Electron Microscope (ThermoFisher Helios G4 PFIB).

Raman spectroscopy was used to investigate the LAGP films using a Horiba Labram Aramis imaging confocal Raman microscope with a 532 nm green laser and collecting spectra over the range 200-1200  $\text{cm}^{-1}$  with an acquisition time of 10 s.

The in-plane ionic conductivity of the films was measured using a Bio-Logic MTZ-35 impedance analyser in the frequency range 0.01 Hz to 10 MHz at an amplitude of 10 mV. Two gold electrodes (1 mm wide and ~30 nm in thickness) were sputtered on the film surfaces with a 1 mm separation. The activation energy for ion conduction was calculated from measurements at 10 °C intervals over the temperature range from 25 °C to 95 °C.

## Results and Discussion

### Phase evolution

Figure 1 shows the XRD patterns of N-doped LAGP thin films deposited on  $\text{Al}_2\text{O}_3$  substrates after annealing at different temperatures. The XRD spectra from as-deposited films only shows the peaks corresponding to the  $\text{Al}_2\text{O}_3$  indicating that the as-deposited films are amorphous. Small peaks corresponding to the LAGP phase appear in the patterns and these peaks become more intense with increasing temperature. Up to 700 °C, the XRD patterns only contain the peaks characteristic of the NASICON structure of LAGP indicating that the films are single-phase with no detectable crystalline impurity phases. At 750 °C new peaks corresponding to  $\text{GeO}_2$  appear in addition to the LAGP peaks. The formation of  $\text{GeO}_2$  in LAGP at high temperatures has been also reported by other authors [30]. The high intensity of the (104) peaks in Figure 1 relative to the values expected from a random polycrystalline sample suggest a mild degree of (104) texture in these films, and this has been confirmed with pole figure analysis.

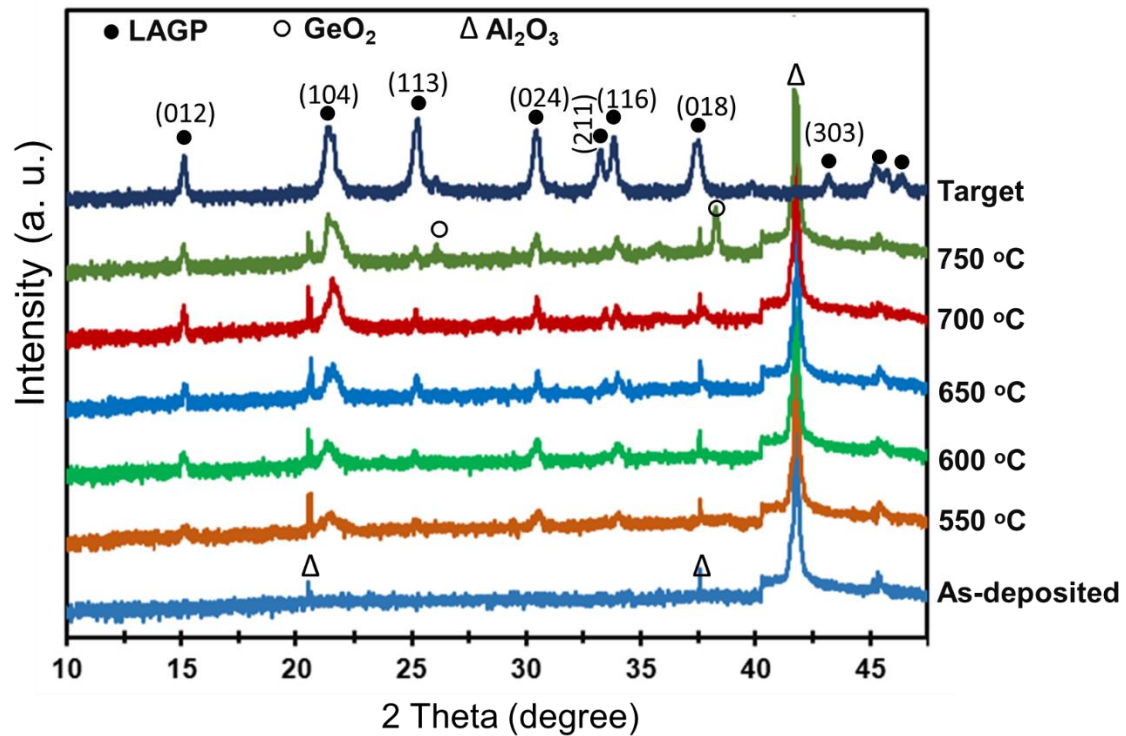


Figure 1. XRD patterns of the N-doped LAGP films deposited on  $\text{Al}_2\text{O}_3$  substrates at  $\text{Ar}+23\%\text{N}_2$  after annealing at various temperatures.

Morphology of the deposited films

The morphology of the top surfaces of LAGP films deposited in different sputtering gas mixtures and crystallised at  $700\text{ }^\circ\text{C}$  is compared in Figure 2. There is not much difference in the surface morphology of films deposited in pure Ar and 15% nitrogen. Both films are relatively smooth, dense and uniform, with no pinholes or cracks, and should be suitable for integrating into battery structures with low contact resistance between the thin film electrolyte and electrode materials and avoiding short circuits.

Increasing the nitrogen content to 30% results in a change in the morphology of the films to a less dense microstructure with a relatively large amount of porosity, and with small needle shaped particles on the surface that are not visible on the films sputtered in lower  $\text{N}_2$  ratios Figure 2c. This might be a result primarily of the lower sputtering rate as the N content in the gas phase increases (as explained below), and could be avoided by sputtering for longer times.

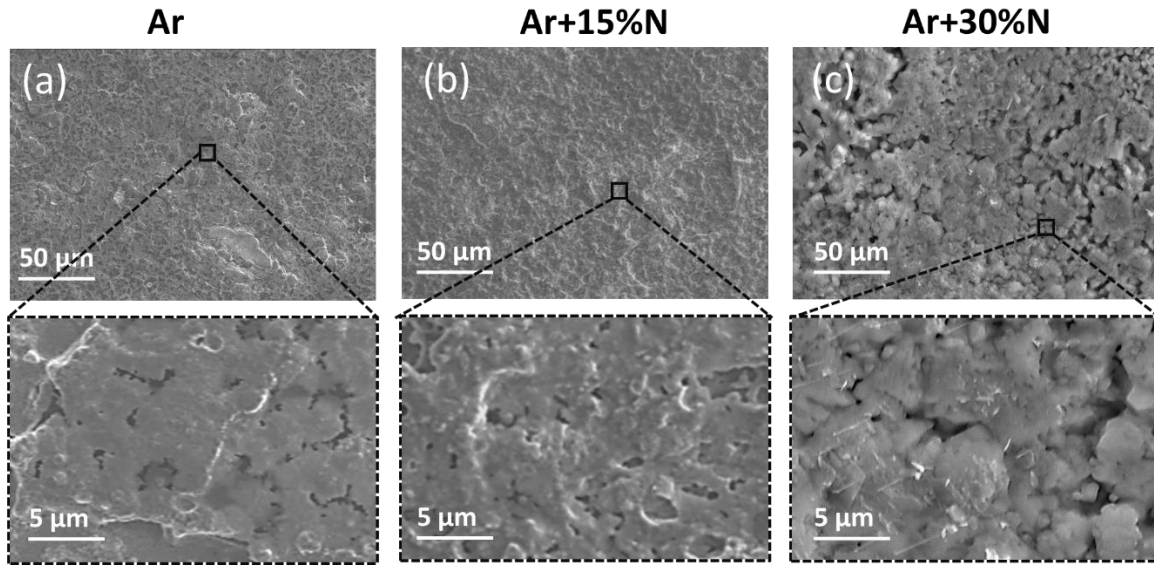


Figure 2. Plan-view SEM images of the LAGP films deposited in various sputtering gas mixtures (a) Pure Ar, (b) Ar+15%N<sub>2</sub> and (c) Ar+30%N<sub>2</sub> and annealed at 700 °C.

Figure 3 shows the morphology of the N-doped LAGP thin films after annealing at various temperatures. The as-deposited films are very flat and featureless as a result of the amorphous structure confirmed by XRD. At temperatures above 550 °C, small crystalline grains are developed, and increasing the annealing temperature to 700 °C results in denser films with well-connected large crystalline grains. However, further increase in annealing temperature leads to a much less uniform microstructure with interconnected porosity, possibly due to the enhanced evaporation of volatile species at higher temperatures. Similar porous microstructures have been observed in N-free LAGP when processed at high temperatures [12], and a study of melt-quenched LAGP during annealing observed Li loss that they attributed to the formation and evaporation of Li<sub>2</sub>O [31]. Since porosity will degrade the ionic conductivity and introduce short circuits in battery structures, it is important to avoid excessively high temperature processing of LAGP thin film solid electrolytes.

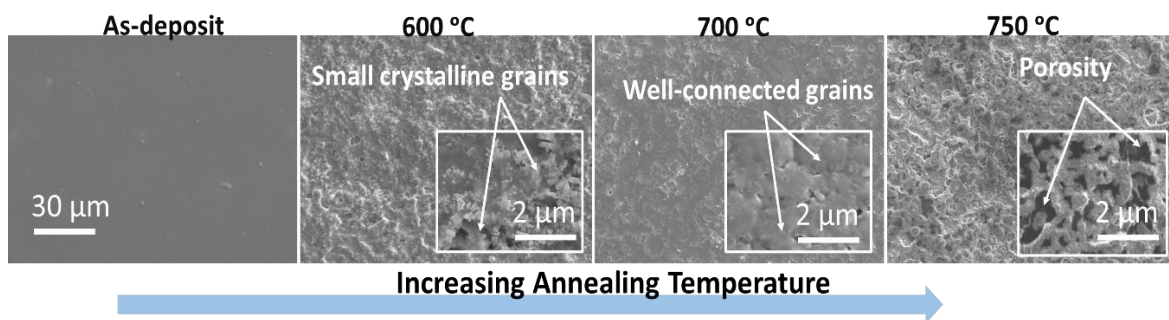


Figure 3. SEM images of the top surface of the N-doped LAGP films deposited on Al<sub>2</sub>O<sub>3</sub> after annealing at various temperatures.

Figure 4 shows cross-sectional images of LAGP thin films deposited on  $\text{Al}_2\text{O}_3$  substrates at different  $\text{Ar}/\text{N}_2$  ratios. Films deposited both in pure Ar and 30% nitrogen contain a significant concentration of pores at least a few hundreds of nm across, but the pores are larger in the N-containing films. It can also be seen that the thickness of the film depends on the  $\text{Ar}/\text{N}_2$  ratio in the sputtering gas. When pure Ar is used, the thickness of the film is about  $1\ \mu\text{m}$  after 6 hrs of sputtering giving a deposition rate of  $155\ \text{nm}/\text{h}$ , but when the nitrogen content in the sputtering gas is increased to 30%, the thickness of the film decreased to about  $850\ \text{nm}$  corresponding to a deposition rate of  $140\ \text{nm}/\text{h}$ . When we take into account the high degree of porosity in these films, the actual deposition rate in  $\text{Ar}+\text{N}$  must be even lower. This can be explained because the heavier the projectile that bombards the atoms in the target, the more efficient is the sputtering process. Decreasing the concentration of Ar ions in the sputtering gas by increasing the  $\text{N}_2$  content is therefore expected to lead to a lower sputtering yield and thinner films. Similar effects of the  $\text{Ar}/\text{N}_2$  ratio on the thickness of films have been reported in other work [32], [33][34].

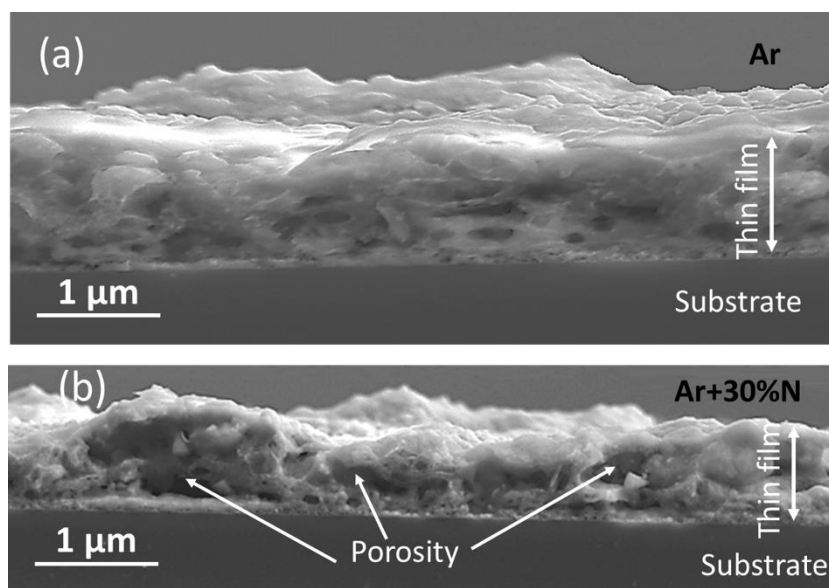


Figure 4. SEM cross-section images of the LAGP thin film deposited in different sputtering gases (a) pure Ar and (b)  $\text{Ar}+30\%\text{N}_2$ .

The cross sectioned samples could also be used for EDX line-scan analysis, avoiding most of the Al signal interference from the sapphire substrate. Figure 5a shows a typical EDX line scan across the LAGP film, and Al, Ge and P can be seen to be fairly uniformly distributed, with no obvious impurity phases. As we have reported before [12], the Al/P and Ge/P ratios are consistent with these ratios in the initial LAGP powder used for the sputtering target, indicating

stoichiometric transfer from target to substrate. Figure 5b also shows elemental maps of the top surface of a thin film reacted at 700 °C. Apart from some increase in the Al counts from the thinner regions of the film, there are no significant local variations in the concentrations of P or Ge. These EDX results demonstrate that the LAGP films are chemically uniform in both cross-sectional and plan views.

We have not shown either the Li or N distributions in these EDX analyses. The absence of data on the Li is due to limitations in the ability of EDX detectors to detect light elements efficiently, but the absence of a strong N signal must be due to this element being present only at low concentration in our LAGP films. Figure 5c shows an EDX spectrum from a relatively large area on the cross-section of the film ( $0.5\mu\text{m}\times 0.5\mu\text{m}$ ), and a small N peak can now be identified. This small N peak was not seen in films deposited in pure Ar indicating that some nitrogen has been incorporated to the LAGP films when deposited in the Ar+N<sub>2</sub> sputtering atmosphere. However the nitrogen content in the film was only ~1 at.% for films deposited at the highest N<sub>2</sub>/Ar ratio (30% N<sub>2</sub>), and may be related either to inefficient incorporation of nitrogen during the sputtering process, and/or preferential loss of nitrogen during the high temperature annealing process required for crystallization.

Nitrogen loss during processing has been also reported in studies on crystalline LiPON. Wang et al found about 75% nitrogen loss in their final product (LiPON bulk) measured from the total weight gain during TGA measurements [18]. In a more recent study by Senevirathne et al [35], it was found that a slight excess of P<sub>3</sub>N<sub>5</sub> precursor was needed in order to compensate for nitrogen loss during the high temperature processing and achieve a single phase Li<sub>2</sub>PO<sub>2</sub>N bulk. Nitrogen loss was less severe in the synthesis of N-doped Li<sub>3</sub>PO<sub>4</sub> compared to N-doped Li<sub>3</sub>VO<sub>4</sub>, and this was suggested to be a result of the lower processing temperature needed for Li<sub>3</sub>PO<sub>4</sub> [36]. In none of the above studies was the actual content of nitrogen in the oxy-nitride produce directly measured, and nitrogen loss was attributed to high-temperature processing and/or decomposition of N-doped product before N-analysis. It is worth mentioning that all these studies are on bulk products, and the nitrogen loss during processing could be even more severe in thin films due to the large surface area.

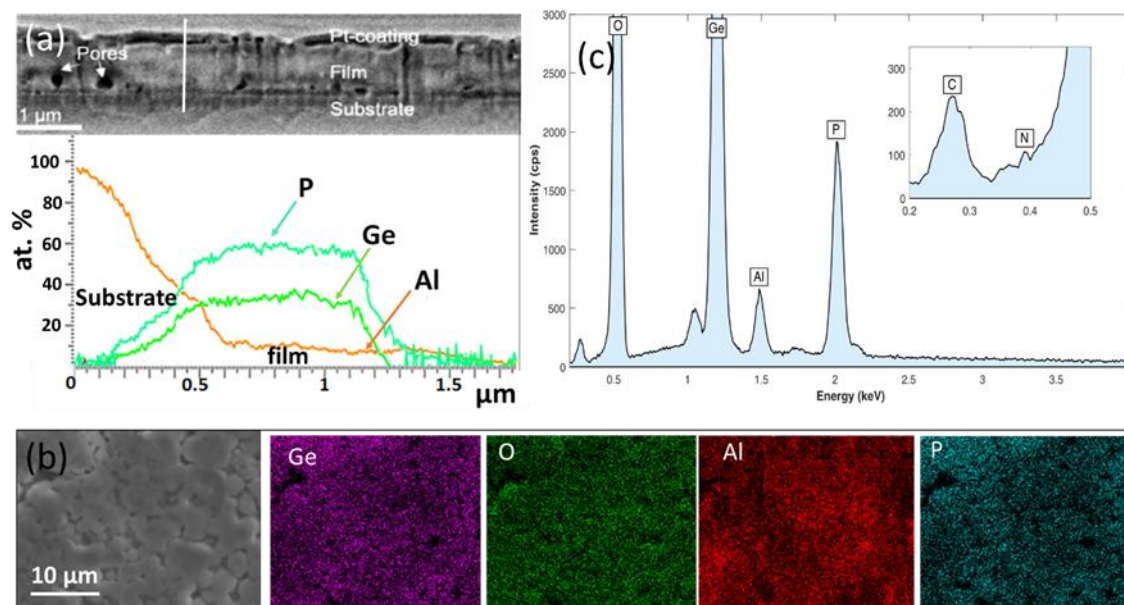


Figure 5. (a) Cross-section of the LAGP thin film deposited on Al<sub>2</sub>O<sub>3</sub> substrate along with an EDX line scan across the LAGP film, (b) Typical elemental maps from the top surface of LAGP thin film. (c) EDX spectrum of an area of the cross section of the film (0.5 $\mu$ m $\times$ 0.5 $\mu$ m).

#### Raman analysis

It has been reported previously that small lattice distortions, not easily observable by XRD, in bulk NASICON-type materials can strongly influence ionic conduction mechanisms [37]. To investigate these small distortions, Raman analysis was carried out for LAGP films deposited in 0% and 22.5% N<sub>2</sub> and annealed at 750 °C. Spectra were taken at 10 positions across the sample surfaces and the normalised intensities were averaged (Figure 6). The main features of these spectra are consistent with NASICON-type compounds with space group  $R\bar{3}c$  [30], [38], but we have to take into account that the intensities of the peaks will be influenced by factors such as film thickness and the presence of surface contamination [39]. For NASICON-type materials, the Raman response is mostly associated with the different vibrational states of the P-O bond in the PO<sub>4</sub> tetrahedra. In the case of LAGP, the PO<sub>4</sub> group provides a link between columns of MO<sub>6</sub> octahedra sharing atoms with the M<sup>3+/4+</sup> and Li<sup>+</sup> ions [40]. The peaks between 850-1200 cm<sup>-1</sup> are associated with the stretching modes of the PO<sub>4</sub> tetrahedra [37], and an obvious change in the spectra in Figure 6 is that the peak shown in the inset shifts in frequency from 1050 cm<sup>-1</sup> for the 0% N<sub>2</sub> sample to 1045 cm<sup>-1</sup> in the presence of N<sub>2</sub>, suggesting the P-O bond has been softened and so stretched by the incorporation into the LAGP of the low concentration of N identified by EDX in Figure 5. There are also peaks at 729 cm<sup>-1</sup> and 749 cm<sup>-1</sup>, indicating the presence of GeO<sub>2</sub> [30] as confirmed by the XRD data in Figure 1.

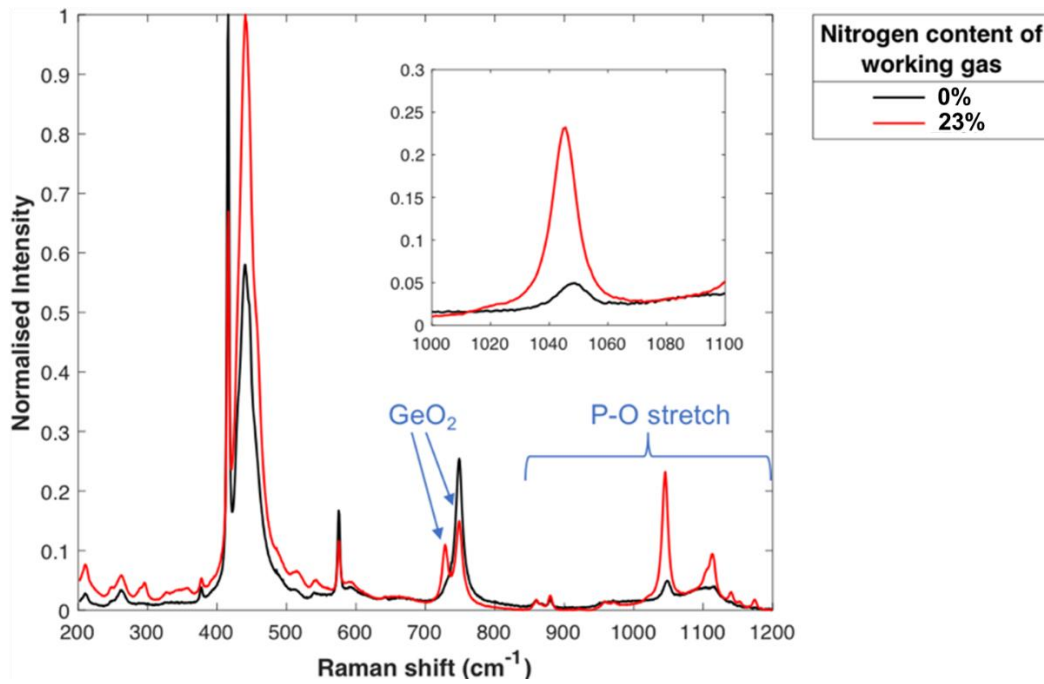


Figure 6. Raman spectra of the LAGP thin films deposited at pure Ar and Ar+23%N<sub>2</sub> and annealed at 750 °C.

Ionic conductivity measurements

EIS measurements were used to determine the in-plane ionic conductivities of these N-doped LAGP films. The as-deposited films showed no ionic conductivity, which is consistent with previous reports on amorphous bulk LAGP [41]. Figure 7 shows typical Nyquist plots at different temperatures for a N-doped LAGP film annealed at 700 °C. All measurements showed a distorted semicircle at high frequencies followed by a straight line at low frequencies, corresponding to the thin film solid electrolyte and blocking electrodes respectively, and the shape of these Nyquist plots is similar to in-plane impedance measurements of solid state electrolyte thin films in the literature [9], [42], [43][44]. A modified Randle circuit has been used to fit these characteristic features [42][45], and the equivalent circuit that fitted our data best (shown in the inset in Figure 7) is composed of a resistor and constant-phase element in parallel ( $R_1//CPE_1$ ) for the depressed semicircle at high frequencies, followed by a resistor ( $R_2$ , charge transfer resistance) and a Warburg element ( $W_{o1}$ , diffusion element) in parallel to a constant-phase element ( $CPE_2$ , double layer capacitance) representing the line at low frequencies. An example of a typical Arrhenius plot to extract the activation energy from measurements at different temperatures is also shown in Figure 7, and a value of 0.374 eV calculated for this film is in good agreement with activation energies for bulk LAGP ceramics reported in the literature (0.35-0.41 eV) [40], [46].

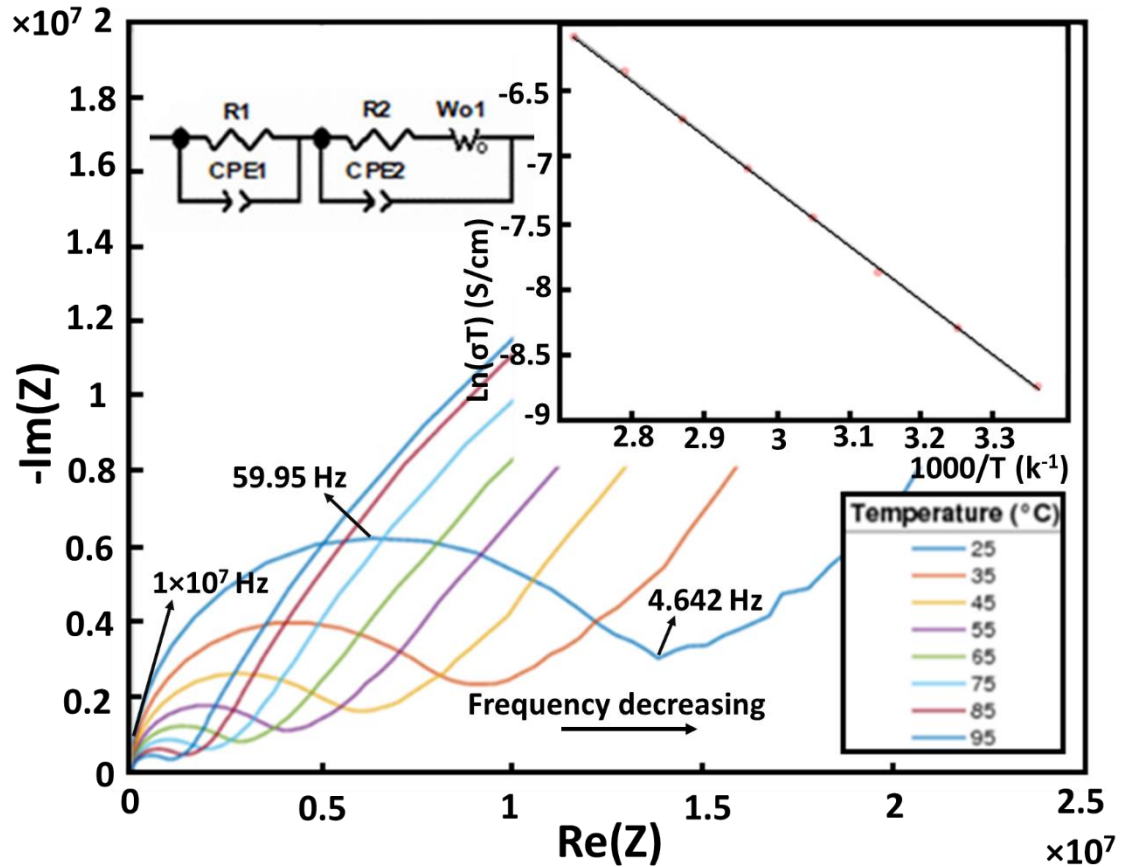


Figure 7. Nyquist plots from a N-doped LAGP film annealed at 700 °C from EIS measurements performed at temperatures between 25 and 95 °C. The insets show the equivalent circuit and an Arrhenius plot of the calculated ionic conductivity as a function of temperature. The capacity value was calculated to be  $2.183E^{-10}$  F at 25 °C.

The ion conductivities and activation energies measured on the N-doped LAGP thin films are plotted in Figure 8 as a function of nitrogen content in the sputtering gas. The ion conductivity is not influenced by nitrogen content in the sputtering gas up to 15%N<sub>2</sub>, but as the nitrogen content increases further, the ionic conductivity increases to a highest value of  $2.3 \times 10^{-4}$  S cm<sup>-1</sup> at 20 °C at a nitrogen content of 23%. The ionic conductivity then decreases with further increase in nitrogen content from 23% to 30%, but even at 30% the ionic conductivity is still higher than the initial value in pure Ar. The peak ionic conductivity achieved for these N-doped LAGP thin films is comparable with the ionic conductivity values reported for LAGP pellets ( $6.76 \times 10^{-4}$  S cm<sup>-1</sup> at 60 °C [5],  $7.25 \times 10^{-4}$  S cm<sup>-1</sup> at room temperature [47]) and for LAGP thick films prepared by tape casting and sintering at 900 °C ( $3.38 \times 10^{-4}$  S cm<sup>-1</sup> at 25 °C) [4], and higher than for undoped LAGP films [11], [12]. The measured activation energies are also lowest (0.374 eV) for the N-doped LAGP film deposited at 23% nitrogen content.

The enhancement of the ionic conductivity by increasing the nitrogen content in sputtering gas may be the result of distortion of some of the PO<sub>4</sub> tetrahedra by partial substitution of O for N changing the structure as suggested by the Raman analysis, although these distortions are not sufficiently severe to be detectable in the XRD analysis. This effect of N opening up the diffusion pathway for Li ions in oxynitrides has been proposed in the literature [48]. It seems necessary to have a significant concentration of nitrogen in the sputtering gas to force enough nitrogen to be incorporated into the structure of the deposited LAGP thin films during deposition. Above a concentration of about 23% the thickness is reduced and the morphology of the films is degraded (as seen in Figure 2 and Figure 4), and the ionic conductivity reduces again.

The presence of pinholes will be particularly problematic for fabricating complete thin film devices where shorts between the electrodes must be avoided. The balance of these two effects leads to the highest improvement in ionic conductivity being found at 23% nitrogen content in the sputtering gas.

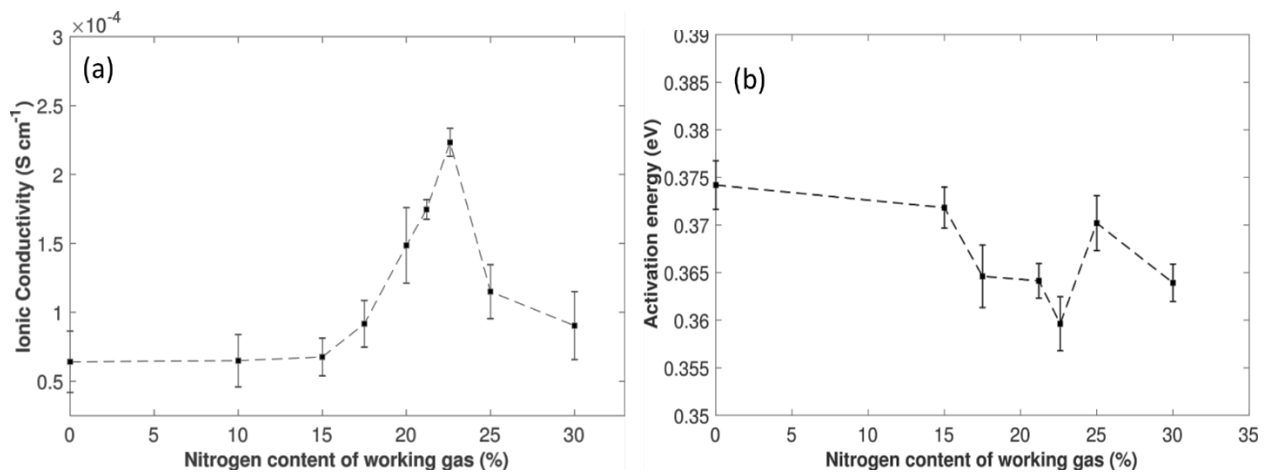


Figure 8. (a) Ionic conductivity and (b) activation energy of N-doped LAGP thin films as a function of nitrogen content in sputtering chamber. The error bars show variation in values measured from at least 3 samples at each condition.

## Conclusions

Nitrogen-doped LAGP thin films can be fabricated by sputtering from LAGP powder targets in a mixture of Ar+N<sub>2</sub> sputtering gas. The ratio of N<sub>2</sub>/Ar was found to be an important factor determining the ionic conductivity of these LAGP solid electrolytes. We have demonstrated that only a low concentration of nitrogen is incorporated into the LAGP structure, but that even at this low level may expand the PO<sub>4</sub> tetrahedral units and encourage more facile Li ion diffusion. However, increasing the nitrogen concentration in the gas phase too far can reduce the deposition rate/thickness of the films and lead to a porous microstructure. The highest ionic conductivity of 2.3×10<sup>-4</sup> S cm<sup>-1</sup> was achieved for N-doped LAGP films containing about 1 at.%

N deposited in mixture of Ar+23%N<sub>2</sub>. This Li<sup>+</sup> conductivity value is very similar to the best achieved in bulk LAGP samples, and is encouraging for considering LAGP as an electrolyte in all thin film battery structures.

**Acknowledgements:** The work reported here was carried out with support from the Faraday Institution [SOLBAT: grant number FIRG007].

## References

- [1] A. Mauger, M. Armand, C. M. Julien, and K. Zaghib, "Challenges and issues facing lithium metal for solid-state rechargeable batteries," *J. Power Sources*, vol. 353, pp. 333–342, 2017.
- [2] C. Sun, J. Liu, Y. Gong, D. P. Wilkinson, and J. Zhang, "Recent advances in all-solid-state rechargeable lithium batteries," *Nano Energy*, vol. 33, pp. 363–386, 2017.
- [3] D. Safanama, D. Damiano, R. Prasada, and S. Adams, "Lithium conducting solid electrolyte Li<sub>1+x</sub>Al<sub>x</sub>Ge<sub>2-x</sub>(PO<sub>4</sub>)<sub>3</sub> membrane for aqueous lithium air battery," *Solid State Ionics*, vol. 262, pp. 211–215, 2014.
- [4] M. Zhang, Z. Huang, J. Cheng, O. Yamamoto, N. Imanishi, and B. Chi, "Solid state lithium ionic conducting thin film Li<sub>1.4</sub>Al<sub>0.4</sub>Ge<sub>1.6</sub>(PO<sub>4</sub>)<sub>3</sub> prepared by tape casting," *J. Alloys Compd.*, vol. 590, pp. 147–152, 2014.
- [5] Y. Zhao, Z. Huang, S. Chen, B. Chen, J. Yang, Q. Zhang, F. Ding, Y. Chen, and X. Xu, "A promising PEO/LAGP hybrid electrolyte prepared by a simple method for all-solid-state lithium batteries," *Solid State Ionics*, vol. 295, pp. 65–71, 2016.
- [6] J. S. Thokchom and B. Kumar, "Composite effect in superionically conducting lithium aluminium germanium phosphate based glass-ceramic," *J. Power Sources*, vol. 185, pp. 480–485, 2008.
- [7] X. Yan, Z. Li, H. Ying, F. Nie, L. Xue, Z. Wen, and W. Han, "A novel thin solid electrolyte film and its application in all-solid-state battery at room temperature," *Ionics (Kiel)*, vol. 24, pp. 1545–1551, 2018.
- [8] D. Ruzmetov, V. P. Oleshko, P. M. Haney, H. J. Lezec, K. Karki, K. H. Baloch, A. K. Agrawal, A. V. Davydov, S. Krylyuk, Y. Liu, J. Huang, M. Tanase, J. Cumings, and A. A. Talin, "Electrolyte stability determines scaling limits for solid-state 3D Li ion batteries," *Nano Lett.*, vol. 12, no. 1, pp. 505–511, 2012.
- [9] S. Lobe, C. Dellen, M. Finsterbusch, H. Gehrke, D. Sebold, and C. Tsai, "Radio frequency magnetron sputtering of Li<sub>7</sub>La<sub>3</sub>Zr<sub>2</sub>O<sub>12</sub> thin films for solid-state batteries," *J. Power Sources*, vol. 307, pp. 684–689, 2016.
- [10] Y. Xiong, H. Tao, J. Zhao, H. Cheng, and X. Zhao, "Effects of annealing temperature on structure and opt-electric properties of ion-conducting LLTO thin films prepared by RF magnetron sputtering," *J. Alloys Compd.*, vol. 509, no. 5, pp. 1910–1914, 2011.
- [11] Z. Sun, L. Liu, B. Yang, Q. Li, B. Wu, J. Zhao, L. Ma, and Y. Liu, "Preparation and ion conduction of Li<sub>1.5</sub>Al<sub>0.5</sub>Ge<sub>1.5</sub>(PO<sub>4</sub>)<sub>3</sub> solid electrolyte films using radio frequency sputtering," *Solid State Ionics*, vol. 346, no. January, p. 115224, 2020.
- [12] T. Mousavi, X. Chen, C. Doerrer, B. Jagger, S. C. Speller, and C. R. M. Grovenor, "Fabrication of Li<sub>1+x</sub>Al<sub>x</sub>Ge<sub>2-x</sub>(PO<sub>4</sub>)<sub>3</sub> thin films by sputtering for solid electrolytes,"

- Solid State Ion.*, vol. 354, no. April, 2020.
- [13] Y. Meesala, A. Jena, H. Chang, and R. S. Liu, "Recent Advancements in Li-Ion Conductors for All-Solid-State Li-Ion Batteries," *ACS Energy Lett.*, vol. 2, no. 12, pp. 2734–2751, 2017.
- [14] F. Zheng, M. Kotobuki, S. Song, M. O. Lai, and L. Lu, "Review on solid electrolytes for all-solid-state lithium-ion batteries," *J. Power Sources*, vol. 389, pp. 198–213, Jun. 2018.
- [15] J. B. Bates, N. J. Dudney, G. R. Gruzalski, R. A. Zuhr, and A. Choudhury, "Fabrication and characterization of amorphous lithium electrolyte thin films and rechargeable thin-film batteries," *J. Power Sources*, vol. 44, pp. 103–110, 1993.
- [16] R. Marchand, D. Agliz, L. Boukbir, and A. Quemerais, "Characterization of nitrogen containing phosphate glasses by X-ray photoelectron spectroscopy," *J. Non. Cryst. Solids*, vol. 103, no. 1, pp. 35–44, Jun. 1988.
- [17] F. Wu, Y. Zheng, L. Li, G. Tan, R. Chen, and S. Chen, "Novel Micronano Thin Film Based on Li – B – P – O Target Incorporating Nitrogen as Electrolyte: How Does Local Structure Influence Chemical and Electrochemical Performances," *J. Phys. Chem. C*, vol. 117, no. 38, p. 19280, 2013.
- [18] B. Wang, B. C. Chakoumakos, B. C. Sales, B. S. Kwak, and J. B. Bates, "Synthesis, Crystal Structure, and Ionic Conductivity of a Polycrystalline Lithium Phosphorus Oxynitride with the  $\gamma$ -Li<sub>3</sub>PO<sub>4</sub> Structure," *J. Solid State Chem.*, vol. 115, no. 2, pp. 313–323, 1995.
- [19] F. Muñoz, "Comments on the structure of LiPON thin-film solid electrolytes," *J. Power Sources*, vol. 198, pp. 432–433, Jan. 2012.
- [20] V. Lacivita, N. Artrith, and G. Ceder, "Structural and Compositional Factors That Control the Li-Ion Conductivity in LiPON Electrolytes," *Chem. Mater.*, vol. 30, pp. 7077–7090, 2018.
- [21] J. M. Kim, G. B. Park, K. C. Lee, H. Y. Park, S. C. Nam, and S. W. Song, "Li-B-O-N electrolytes for all-solid-state thin film batteries," *J. Power Sources*, vol. 189, no. 1, pp. 211–216, 2009.
- [22] K. H. Joo, H. J. Sohn, P. Vinatier, B. Pecquenard, and A. Levasseur, "Lithium ion conducting lithium sulfur oxynitride thin film," *Electrochem. Solid-State Lett.*, vol. 7, no. 8, pp. 256–259, 2004.
- [23] F. Michel, F. Kuhl, M. Becker, J. Janek, and A. Polity, "Electrochemical and Optical Properties of Lithium Ion Conducting LiPSON Solid Electrolyte Films," *Phys. Status Solidi Basic Res.*, vol. 256, no. 10, pp. 1–6, 2019.
- [24] C. Park, S. Lee, S. Choi, and D. Shin, "Effect of boron/phosphorus ratio in lithium boron phosphorus oxynitride thin film electrolytes for all-solid-state thin film batteries," *Thin Solid Films*, vol. 685, no. June, pp. 434–439, 2019.
- [25] S. J. Lee, J. H. Bae, H. W. Lee, H. K. Baik, and S. M. Lee, "Electrical conductivity in Li-Si-P-O-N oxynitride thin-films," *J. Power Sources*, vol. 123, no. 1, pp. 61–64, 2003.
- [26] T. Famprakis, J. Galipaud, O. Clemens, B. Pecquenard, and F. Le Cras, "Composition Dependence of Ionic Conductivity in LiSiPO(N) Thin-Film Electrolytes for Solid-State Batteries," *ACS Appl. Energy Mater.*, vol. 2, no. 7, pp. 4782–4791, 2019.
- [27] G. Tan, F. Wu, L. Li, Y. Liu, and R. Chen, "Magnetron Sputtering Preparation of Nitrogen-Incorporated Lithium – Aluminum – Titanium Phosphate Based Thin Film Electrolytes for All-Solid-State Lithium Ion Batteries," *J. Phys. Chem. C*, vol. 116, no. 5, p. 3817, 2012.
- [28] T. Mousavi, C. Grovenor, and S. Speller, "Characterization of superconducting Fe<sub>1-x</sub>Te<sub>x</sub> thin films deposited on MgO substrates by sputtering," *J. Mater. Sci.*, vol. 50, no. 21, pp. 6970–6978, 2015.

- [29] T. Mousavi, C. Grovenor, and S. Speller, "Effects of Processing Condition on the Properties of Fe ( Se , Te ) Thin Films Grown by Sputtering," *IEEE Trans. Appl. Supercond.*, vol. 25, no. 3, p. 750064, 2015.
- [30] S. V Pershina, A. A. Pankratov, E. G. Vovkotrub, and B. D. Antonov, "Promising high-conductivity  $\text{Li}_{1.5}\text{Al}_{0.5}\text{Ge}_{1.5}(\text{PO}_4)_3$  solid electrolytes: the effect of crystallization temperature on the microstructure and transport properties," *Ionics (Kiel)*, vol. 25, no. 10, pp. 4713–4725, 2019.
- [31] Y. Zhu, Y. Zhang, and L. Lu, "Influence of crystallization temperature on ionic conductivity of lithium aluminum germanium phosphate glass-ceramic," *J. Power Sources*, vol. 290, pp. 123–129, 2015.
- [32] S. Zhang, F. Yan, Y. Yang, M. Yan, Y. Zhang, and J. Guo, "Applied Surface Science Effects of sputtering gas on microstructure and tribological properties of titanium nitride films," *Appl. Surf. Sci.*, vol. 488, no. May, pp. 61–69, 2019.
- [33] F. Anjum, R. Ahmad, and N. Afzal, "Influence of sputtering power and Ar – N<sub>2</sub> flow on the structure and optical properties of indium nitride films prepared by magnetron sputtering," *Radiat. effects Defects*, vol. 174, no. 9, p. 828, 2019.
- [34] T. Mousavi, Z. Hong, A. Morrison, and A. London, "A new approach to fabricate superconducting NbTi alloys," *Supercond. Sci. Technol.*, vol. 30, p. 094001, 2017.
- [35] K. Senevirathne, C. S. Day, M. D. Gross, A. Lachgar, and N. A. W. Holzwarth, "A new crystalline LiPON electrolyte: Synthesis, properties, and electronic structure," *Solid State Ionics*, vol. 233, pp. 95–101, 2013.
- [36] L. Vo, B. Dong, R. Jarkaneh, S. Hull, N. Reeves-mclaren, J. Jacas, and A. R. West, "Synthesis , structure and electrical properties of N-doped  $\text{Li}_3\text{VO}_4$ ," *J. Mater. Chem. A*, no. 4, pp. 1408–1413, 2016.
- [37] B. E. Francisco and C. R. Stoldt, "Lithium-Ion Trapping from Local Structural Distortions in Sodium Super Ionic Conductor (NASICON) Electrolytes," *Chem. Mater.*, vol. 26, no. 16, p. 4741, 2014.
- [38] À. Ge and S. Adams, "Structural evolution of NASICON-type  $\text{Li}_{1+x}\text{Al}_x\text{Ge}_{2-x}(\text{PO}_4)_3$  using in situ synchrotron X-ray powder diffraction," *J. Mater. Chem. A*, vol. 1, no. 20, pp. 7718–7726, 2016.
- [39] K. Bakeev, *Process Analytical Technology: Spectroscopic Tools and Implementation Strategies for the Chemical and Pharmaceutical Industries*. Wiley, 2010.
- [40] D. Safanama, N. Sharma, R. P. Rao, H. E. A. Brand, and S. Adams, "Structural evolution of NASICON-type  $\text{Li}_{1+x}\text{Al}_x\text{Ge}_{2-x}(\text{PO}_4)_3$  using in situ synchrotron X-ray powder diffraction," *J. Mater. Chem. A*, vol. 4, no. 20, pp. 7718–7726, 2016.
- [41] M. Kotobuki and M. Koishi, "Preparation of  $\text{Li}_{1.5}\text{Al}_{0.5}\text{Ge}_{1.5}(\text{PO}_4)_3$  solid electrolytes via the co-precipitation method," *J. Asian Ceram. Soc.*, vol. 7, no. 4, pp. 551–557, 2019.
- [42] T. Kelly, B. M. Ghadi, S. Berg, and H. Ardebili, "In Situ Study of Strain-Dependent Ion Conductivity of Stretchable Polyethylene Oxide Electrolyte," *Sci. Rep.*, vol. 6, p. 20128, Feb. 2016.
- [43] I. Garbayo, M. Struzik, W. J. Bowman, R. Pfenninger, E. Stilp, and J. L. M. Rupp, "Glass-Type Polyamorphism in Li-Garnet Thin Film Solid State Battery Conductors," *Adv. Energy Mater.*, vol. 1702265, pp. 1–14, 2018.
- [44] S. Sabooni, T. Mousavi, and F. Karimzadeh, "Thermodynamic analysis and characterisation of nanostructured Cu(Mo) compounds prepared by mechanical alloying and subsequent

- sintering,” *Powder Metall.*, vol. 55, no. 3, pp. 222–227, 2012.
- [45] J. Wei, D. Ogawa, T. Fukumura, Y. Hirose, and T. Hasegawa, “Epitaxial strain-controlled ionic conductivity in li-ion solid electrolyte  $\text{Li}_{0.33}\text{La}_{0.56}\text{TiO}_3$  thin films,” *Cryst. Growth Des.*, vol. 15, no. 5, pp. 2187–2191, 2015.
- [46] M. Zhang, K. Takahashi, N. Imanishi, Y. Takeda, O. Yamamoto, B. Chi, J. Pu, and J. Li, “Preparation and Electrochemical Properties of  $\text{Li}_{1+x}\text{Al}_x\text{Ge}_{2-x}(\text{PO}_4)_3$  Synthesized by a Sol-Gel Method,” *J. Electrochem. Soc.*, vol. 159, no. 7, pp. A1114–A1119, 2012.
- [47] X. Xu, Z. Wen, X. Wu, X. Yang, and Z. Gu, “Lithium ion-conducting glass-ceramic of  $\text{Li}_{1.5}\text{Al}_{0.5}\text{Ge}_{1.5}(\text{PO}_4)_3x\text{Li}_2\text{O}$  with good electrical and electrochemical properties,” *J. Am. Ceram. Soc.*, vol. 90, no. 9, pp. 2802–2806, 2007.
- [48] Y. A. Du and N. A. W. Holzwarth, “First-principles study of LiPON and related solid electrolytes,” *Phys. Rev. B*, vol. 81, no. 18, p. 184106, May 2010.